ISSN 0915-633X

NATIONAL INSTITUTE FOR FUSION SCIENCE

Effects of Multiple-Helicity Fields on Ion Temperature Gradient Modes

T. Kuroda and H. Sugama

(Received - Mar. 9, 2001)

NIFS-687 Apr. 2001

RESEARCH REPORT
NIFS Series

TOKI, JAPAN

Effects of Multiple-Helicity Fields on Ion Temperature Gradient Modes

T. KURODA and H. SUGAMA[1,2]

[1] *National Institute for Fusion Science, Toki 509-5292*
[2] *Graduate University for Advanced Studies, Toki 509-5292*

(Received March 8, 2001)

Effects of multiple-helicity magnetic fields on ion temperature gradient (ITG) modes in toroidal helical systems like the Large Helical Device (LHD) are studied by means of the linear gyrokinetic theory. Especially, dependence of the real frequency, growth rate, and the eigenfunction of the ITG mode on sideband-helicity fields added to the main helical component is investigated. Comparison between multiple-helicity effects on the ITG mode with those on the neoclassical ripple transport is presented, and optimization of the magnetic configuration for better plasma confinement is discussed.

KEYWORDS. ITG mode, helical system, gyrokinetic equation, multiple helicity

Many theoretical studies have been done on the ion temperature gradient (ITG) modes[1,2] as a cause of anomalous ion heat transport in tokamak plasmas. Also, recently, several works[3–7] have begun to investigate the ITG modes in helical systems since high ion temperature plasmas with $T_i(0) \sim 3.5$ keV[8] were experimentally produced in such systems as the Large Helical Device (LHD) of the National Institute of Fusion Science.[9] The helical systems can make various three-dimensional configurations with different helical magnetic components, which influences plasma stabilities and transport processes. In our previous paper,[3] we treated the ITG modes in the LHD-like helical configuration, where we used a simple model of the magnetic field strength with a toroidal component and a single helical component. In the present work, we investigate how linear properties of the ITG modes are affected by addition of multiple-helicity fields. So far, multiple-helicitiy effects on the neoclassical ripple transport have already been systematically analyzed by several authors.[10–12] Then, it is meaningful to compare the multiple-helicity effects on the ITG modes with those on the neoclassical transport from the point of view of optimizing the magnetic configurations for better confinement of helical plasmas. Such a comparison is also presented in this report.

Here, we use the following model of the magnetic field strength B,

$$B/B_0 = 1 - \epsilon_t \cos\theta - \epsilon_h \cos(L\theta - M\zeta) - \epsilon_- \cos[(L-1)\theta - M\zeta] - \epsilon_+ \cos[(L+1)\theta - M\zeta] \quad (1)$$

where B_0 is the magnitude on the magnetic axis, θ and ζ denote the poloidal and toroidal angles, respectively, and M (L) is the toroidal (main poloidal) period number of the helical fields. For the LHD, $L = 2$ and $M = 10$. Here, $\epsilon_t(r) = r/R \ll 1$ (r: the minor radius, R: the major radius) and $\epsilon_h(r) \propto r^L$ are the parameters associated with the toroidicity and the main helical component, respectively, while $\epsilon_-(r) \propto r^{L-1}$ and $\epsilon_+(r) \propto r^{L+1}$ represent sideband helical components. For example, the absolute values of ϵ_+ and ϵ_- become large when the magnetic axis is shifted from the standard position by changing the vertical field.[13]

We use a kinetic integral equation to obtain the linear dispersion relation and the mode structure of the ITG mode in the same way as in ref. 3 (see also refs. 14–16). The kinetic integral equation is derived from using the collisionless ion gyrokinetic equation,[17,18] the adiabatic electron assumption, and the quasineutrality condition in the ballooning representation.[19,20] Effects of the magnetic configuration are taken into account only through the ∇B-curvature drift frequency term in the ion gyrokinetic equation. Trapped particle effects are neglected here since mainly the passing ions drive the ITG modes. For the magnetic field strength given by eq. (1), the ion ∇B-curvature drift frequency is given by

$$\omega_D = 2(L_n/r)\,\epsilon_t \omega_{*i}\,(v_\parallel^2 + v_\perp^2/2)\, v_{Ti}^{-2}\, G_c(\theta) \quad (2)$$

with the curvature factor,

$$G_c(\theta) = \cos\theta + \hat{s}(\theta - \theta_k)\sin\theta + \sum_{l=L-1}^{L+1} l\,(\epsilon_l/\epsilon_t)\Big[\cos((l - Mq)\theta - M\alpha) + \hat{s}(\theta - \theta_k)\sin((l - Mq)\theta - M\alpha)\Big], \quad (3)$$

where $\epsilon_L = \epsilon_h$, $\epsilon_{L-1} = \epsilon_-$, and $\epsilon_{L+1} = \epsilon_+$. Here, $L_n \equiv -n_0[dn_0(r)/dr]^{-1}$ is the background density scale length, $\omega_{*i} \equiv -\tau_e^{-1}\omega_{*e}$ is the ion diamagnetic drift frequency, $\tau_e \equiv T_e/T_i$ is the ratio between the electron and ion temperatures, $\omega_{*e} \equiv ck_\theta T_e/(eBL_n)$ (k_θ: the poloidal wavenumber) is the electron diamagnetic drift frequency, $v_\parallel$ ($v_\perp$) is the ion parallel (perpendicular) velocity, $v_{Ti} \equiv (2T_i/m_i)^{1/2}$ is the ion thermal velocity, $\hat{s} = (r/q)dq/dr$ (q: the safety factor) is the magnetic shear parameter, θ_k is the poloidal angle parameter associated with the ballooning representation, and $\alpha = \zeta - q\theta$ is the label of the magnetic field line. The curvature factor $G_c(\theta)$ represents the structure of the ∇B-curvature

drift frequency along the magnetic field line. Since, in the ballooning representation, the poloidal angle variable θ is used as a coordinate along the field line, $G(\theta)$ is not a periodic function of θ but a function defined on the so-called covering space, $-\infty < \theta < \infty$.[19,20] It should be noted that $G_c(\theta) > 0$ (< 0) corresponds to bad (good) curvature regions, where destabilization (stabilization) of the modes occurs.

The kinetic integral equation for the electrostatic potential ϕ, which contains a complex-valued frequency $\omega = \omega_r + i\gamma$ as an eigenvalue, is written as[3,15]

$$\left(1+\frac{T_e}{T_i}\right)\phi(\omega,k) = \int_{-\infty}^{+\infty}\frac{dk'}{\sqrt{2\pi}}K(k,k')\phi(\omega,k') \quad (4)$$

with

$$K(k,k') = -\mathrm{i}\int_{-\infty}^{0}\omega_{*e}d\tau\frac{\sqrt{2}e^{-\mathrm{i}\omega\tau}}{\sqrt{a}(1+a)\sqrt{\lambda}}e^{-(k-k')^2/4\lambda}$$
$$\times\left[\frac{\omega}{\omega_{*e}}\tau_e + 1 - \frac{3}{2}\eta_i + \frac{\eta_i(k-k')^2}{4a\lambda} + \right.$$
$$\left.\frac{2\eta_i}{(1+a)}\left(1 - \frac{k_\perp^2+k_\perp'^2}{2(1+a)\tau_e} + \frac{k_\perp k_\perp'}{(1+a)\tau_e}\frac{I_1}{I_0}\right)\right]\Gamma_0(k_\perp,k_\perp'), \quad (5)$$

where $I_j = I_j(k_\perp k_\perp'/[(1+a)\tau_e])$ $(j = 0,1)$ are the modified Bessel functions of j-th order, $\eta_i = (d\ln T_i/dr)/(d\ln n_0/dr)$, $\lambda = (\omega_{*e}\tau)^2(\hat{s}\epsilon_n/q)^2/\tau_e a$, $\epsilon_n = L_n/R$, $k = \hat{s}k_\theta(\theta-\theta_k)$, $k' = \hat{s}k_\theta(\theta'-\theta_k)$, $\Gamma_0(k_\perp,k_\perp') = I_0(\ k_\perp k_\perp'/[(1+a)\tau_e]\ )\exp[-(k_\perp^2+k_\perp'^2)/2\tau_e(1+a)]$, $k_\perp^2 = k_\theta^2+k^2$, and $k_\perp'^2 = k_\theta^2+k'^2$. Here, the wavenumber variables k_θ, k, and k' are normalized by ρ_s^{-1} ($\rho_s = \sqrt{2T_e/m_i}/\Omega_i = \tau_e^{1/2}\rho_{Ti}$). The effects of the ∇B-curvature drift frequency given by eqs. (2) and (3) are included in the kernel $K(k,k')$ through the variable a defined by

$$a = 1 + \mathrm{i}\frac{\tau}{\theta-\theta'}\int_{\theta'}^{\theta}d\theta''\omega_D(\theta'')$$
$$= 1 - \mathrm{i}2(L_n/r)\tau_e^{-1}\omega_{*e}\tau/(\theta-\theta')$$
$$\times\Bigg(\quad\epsilon_t\Big[\,(\hat{s}+1)(\sin\theta-\sin\theta')$$
$$-\hat{s}\{(\theta-\theta_k)\cos\theta-(\theta'-\theta_k)\cos\theta'\}\,\Big]$$
$$+\sum_{l=L-1}^{L+1}l\,\frac{\epsilon_l}{l-Mq}\Bigg[\quad\left(\frac{\hat{s}}{l-Mq}+1\right)$$
$$\times\Big\{\,\sin[(l-Mq)\theta-M\alpha]$$
$$-\sin[(l-Mq)\theta'-M\alpha]\,\Big\}$$
$$-\hat{s}\Big\{\,(\theta-\theta_k)\cos(\ (l-Mq)\theta-M\alpha\ )$$
$$-(\theta'-\theta_k)\cos(\ (l-Mq)\theta'-M\alpha\ )\,\Big\}\quad\Bigg]\quad\Bigg). \quad (6)$$

Hereafter, results from numerical solution of the integral equation (4) with the boundary conditions $\phi(\theta\to\pm\infty) = 0$ are shown for the helical system with $L = 2$ and $M = 10$ (corresponding to the LHD case). Our numerical code can calculate both positive and negative growth rates with proper analytic continuation of the dispersion relation in the complex frequency plane.[21-23] Detailed procedures for the analytic continuation are shown in ref. 23. Parameters used here are the same as the standard parameters in ref. 3 (see Table I) except for ϵ_+ and ϵ_-. The standard parameters q, $\hat{s}$, θ_k, α, and ϵ_h/ϵ_t in Table I are chosen such that they correspond to the mode localized in the outside of the torus along the field line, which passes through the point with the lowest magnetic field strength on the magnetic surface $r/a = 0.6$ of the LHD plasma. In Table I, $k_\theta\rho_{Ti} = 0.65$ is the normalized poloidal wavenumber, which correspond to the largest growth rate for the case of no sideband components, $\epsilon_+ = \epsilon_- = 0$ (see Fig. 10 in ref. 3).

Table I. Standard parameters

q	$\hat{s}$	θ_k	α	$k_\theta\rho_{Ti}$	η_i	ϵ_n	τ_e	ϵ_h/ϵ_t	L	M
2	−1	0	0	0.65	3	0.3	1	1	2	10

Figure 1 shows effects of the sideband helical ripple parameters ϵ_+/ϵ_t and ϵ_-/ϵ_t on the normalized real frequency ω_r/ω_{*e} and the normalized growth rate γ/ω_{*e} of the ITG mode. The growth rate depends on the sideband helical components more strongly than the real frequency. In order to see more clearly the sideband-helicity dependence of the growth rate, we plot in Fig. 2 contours of the normalized growth rate $\hat{\gamma} \equiv \gamma/\gamma_{00}$ on the $(\epsilon_-/\epsilon_t, \epsilon_+/\epsilon_t)$-plane, where $\gamma_{00} = 0.183\omega_{*e}$ is the growth rate for the case of $\epsilon_+ = \epsilon_- = 0$. The stable region ($\gamma < 0$) appears for large ϵ_+, and the peak of growth rate ($\hat{\gamma} = 1.5$) exist at $(\epsilon_-/\epsilon_t, \epsilon_+/\epsilon_t) = (-1.0, -0.4)$.

It is interesting to compare the effects of the sideband helical components on the ITG mode shown above with their effects on the neoclassical transport. For this purpose, we use the geometrical factor for the neoclassical ripple transport,[11,12] which is given by $G_{\rm neo} = \int_0^{2\pi}d\theta\,\epsilon_H^{3/2}\,[G_1(\partial\epsilon_T/\partial\theta)^2 - 2G_2(\partial\epsilon_T/\partial\theta)(\partial\epsilon_H/\partial\theta) + G_3(\partial\epsilon_H/\partial\theta)^2]$ with $G_1 = 16/9$, $G_2 = 16/15$, and $G_3 = 0.684$. Here, $\epsilon_T = -\epsilon_t\cos\theta$, $\epsilon_H = (C^2+D^2)^{1/2}$, $C = -\epsilon_h - (\epsilon_+ + \epsilon_-)\cos\theta$, and $D = -(\epsilon_+ - \epsilon_-)\sin\theta$ for the magnetic field strength given by eq. (1). Figure 3 shows contours of the normalized geometrical factor $\hat{G}_{\rm neo} \equiv G_{\rm neo}/(G_{\rm neo})_{00}$ on the $(\epsilon_-/\epsilon_t, \epsilon_+/\epsilon_t)$-plane, where $(G_{\rm neo})_{00}$ represents the value of $G_{\rm neo}$ for $\epsilon_+ = \epsilon_- = 0$. We see from Figs. 2 and 3 that the sideband-helicity parameters around the peak of the growth rate ($\hat{\gamma} = 1.5$) correspond to a dip of the neoclassical geometrical factor ($\hat{G}_{\rm neo} < 1$), and that the stable region for the ITG mode ($\hat{\gamma} < 0$) gives the large neoclassical transport ($\hat{G}_{\rm neo} \geq 3$).

In order to physically understand the relation between the ITG mode, the neoclassical transport, and the magnetic structure, we plot the eigenfunction $\phi(\theta) = \phi_r + \mathrm{i}\phi_i$ of the ITG mode, the curvature factor $G_c(\theta)$, and the magnetic field strength $B(\theta)$ along the field line for

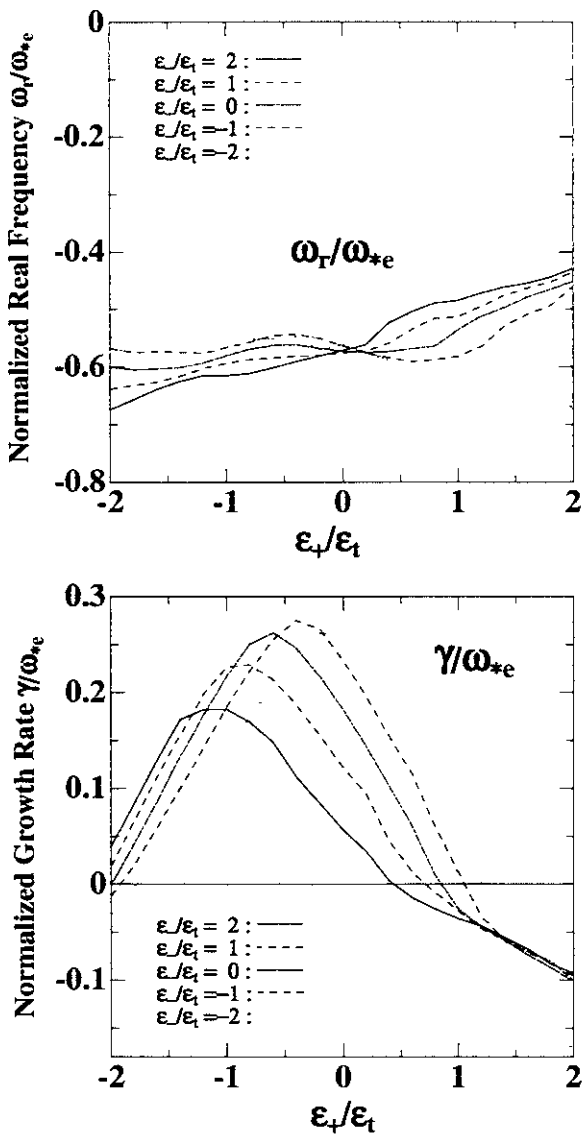

Fig 1. Effects of ϵ_+/ϵ_t and ϵ_-/ϵ_t on the normalized real frequency ω_r/ω_{*e} and the normalized growth rate γ/ω_{*e} of the ITG mode.

$(\epsilon_-/\epsilon_t, \epsilon_+/\epsilon_t) = (0.0)$, $(-1, -0.4)$ $(-0.4, -2)$, $(1, -0.8)$, and $(1, 1)$, in Figs. 4 (a), (b), (c), (d), and (e), respectively. For convenience, these sideband-helicity parameters for Figs. 4 (a)–(e) are plotted by the crosses labeled as a–e on the $(\epsilon_-/\epsilon_t, \epsilon_+/\epsilon_t)$-plane in Figs. 2 and 3, respectively. Using the normalized parameters $\hat{G}_{\rm neo}$ and $\hat{\gamma}$, we obtain $(\hat{\gamma}, \hat{G}_{\rm neo}) = (1, 1)$ for Fig. 4 (a), $= (1.5, 0.177)$ for (b), $= (-0.019, 0.54)$ for (c), $= (1.25, 3.59)$ for (d), and $= (-0.151, 7.03)$ for (e). Then, a larger ITG mode growth rate and a smaller neoclassical (NCL) transport are given for the case of Fig. 4 (b) than for the case of no sideband components in Fig. 4 (a), which is denoted by (ITG, NCL) = (bad, good) for (b). In the same way, the rest of combinations (ITG, NCL) = (good, good), (bad, bad), and (good,bad) are given for (c), (d), and (e), respectively.

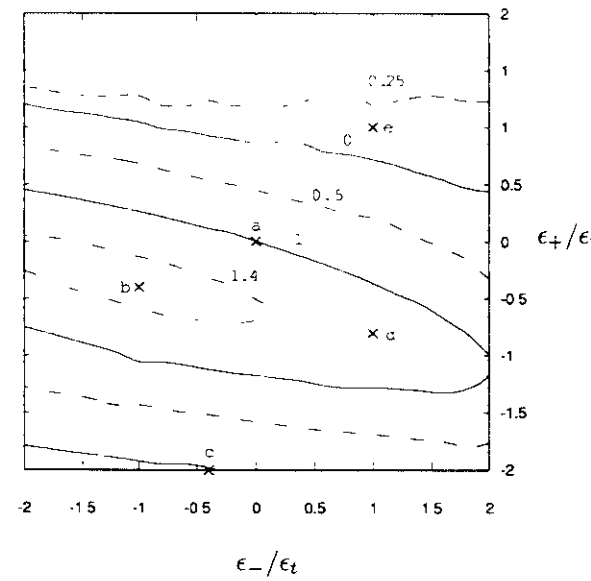

Fig. 2. Contours of the normalized growth rate $\hat{\gamma} \equiv \gamma/\gamma_{00}$ on the $(\epsilon_-/\epsilon_t, \epsilon_+/\epsilon_t)$-plane. Here $\gamma_{00} = 0.183\omega_{*e}$ is the growth rate for the case of $\epsilon_+ = \epsilon_- = 0$.

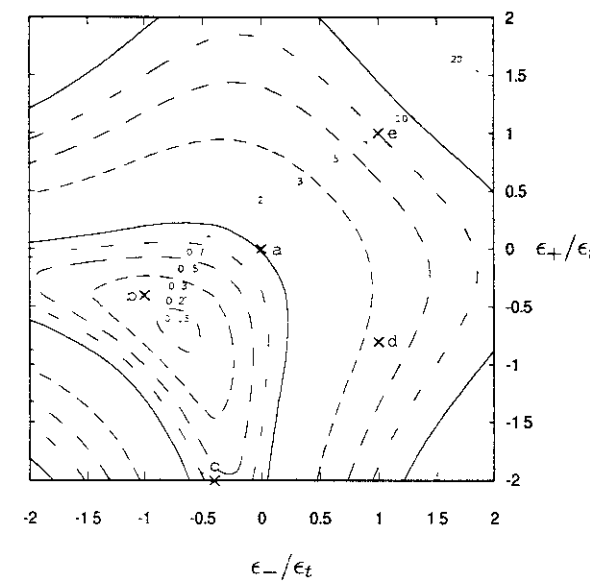

Fig 3. Contours of the normalized geometrical factor $\hat{G}_{\rm neo}$ for the neoclassical ripple transport on the $(\epsilon_-/\epsilon_t, \epsilon_+/\epsilon_t)$-plane. Here, $\hat{G}_{\rm neo} = 1$ for $\epsilon_+ = \epsilon_- = 0$

We see from the profile $B(\theta)/B_0$ in Fig. 4 that the bottom of the magnetic ripple is nearly constant in the case of (b). This magnetic profile is favorable from the viewpoint of neoclassical transport because deviations of orbits of deeply trapped particles from magnetic surfaces are small for such a profile.[10–12] Also, in the case of (b),

the profile of $G_c(\theta)$ have a clear bad curvature region in the outside of the torus ($-\pi/2 < \theta < \pi/2$) like that for the tokamak case. Then, the eigenfunction $\phi(\theta)$ resembles that in the negative-shear tokamak case (see Fig. 2 in ref. 3), and the growth rate is larger than in the no sideband-helicity case of (a).

In the case of (c), $B(\theta)$ has nearly constant bottoms like in the case of (b), while $G_c(\theta)$ gives larger amplitude oscillations than for (a). Then, significant good curvature regions also exist around $\theta \sim 0$, which is favorable from the viewpoint of the ITG mode stabilization. Consequently, a lower ITG growth rate and smaller neoclassical transport are simultaneously realized for (c) than for (a).

For (d) and (e), the bottom of magnetic ripple is far from constant and is unfavorable for neoclassical transport. The curvature factor $G_c(\theta)$ has small but positive values around $\theta \sim 0$ for (d) while it has large oscillations around $\theta \sim 0$ for (e) like for (c). Thus, we have (ITG, NCL) = (bad, bad) for (d), and (good, bad) for (e).

Here, it is recalled that $\theta_k = 0$ and $\alpha = 0$ are used for the calculations in Figs. 1–4. For the multiple-helicity fields considered here, we have also confirmed stabilizing effects of increasing $|\theta_k|$ and weak dependence of the linear ITG mode properties on α in the same way as in ref. 3 (see Figs. 7 and 8 in ref. 3).

In summary, this work have shown how the ITG mode properties depend on the sideband components of the multiple-helicity fields in the LHD-like helical system. Effects of the multiple-helicity fields on the ITG mode are compared with those on the neoclassical ripple transport. Mechanisms of these effects are physically explained from profiles of the curvature factor $G_c(\theta)$ and the magnetic field strength $B(\theta)$ along the field line. Adjustment of these profiles as shown in Fig. 4(c) can reduce the ITG mode growth rate and the neoclassical ripple transport simultaneously, which may give a clue for optimization of the magnetic field configuration for better plasma confinement. It should be noted that the linear ITG mode analysis here have neglected effects of trapped particles, which may affect the ITG mode growth rate. Also, effects of collisions, nonadiabatic electrons, impurities, magnetic fluctuations, and sheared radial electric fields have not been taken into account. Investigation of these effects remains as future tasks.

Acknowledgements

The authors thank Dr. M. Yokoyama for useful discussions and comments on the multiple-helicity fields. They also appreciate continuous encouragement of this work by Dr. R. Kanno, Prof. M. Okamoto, and Prof. K. Itoh. Numerical calculations in this study are performed on the computer system of the Computer Center in the National Institute for Fusion Science. This work is supported in part by the Grant-in-Aid from the Japanese Ministry of Education, Culture, Sports, Science and Technology, No. 12680497.

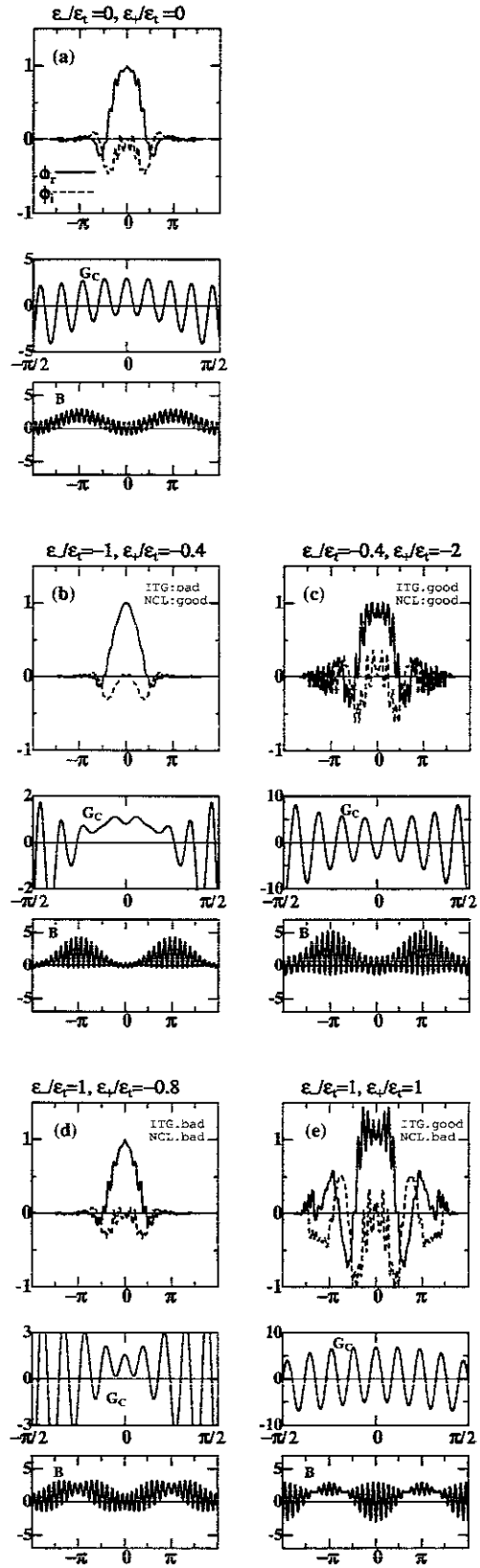

Fig. 4. The eigenfunction $\phi(\theta) = \phi_r + i\phi_i$ of the ITG mode, the curvature factor $G_c(\theta)$, and the magnetic field strength $B(\theta)/B_0$ along the field line. Here, $(\epsilon_-/\epsilon_t, \epsilon_+/\epsilon_t) = (0, 0)$ for (a), $(-1, -0.4)$ for (b), $(-0.4, -2)$, for (c), $(1, -0.8)$, for (d), and $(1, 1)$ for (e), which correspond to the crosses labeled as a, b, c, d, and e in Figs. 2 and 3, respectively. Note that only $G_c(\theta)$ is plotted in the range $-\pi/2 \leq \theta \leq \pi/2$, where $\phi(\theta)$ is dominantly localized.

1) W. Horton: Rev. Mod. Phys. **71** (1999) 735.
2) W. Horton, M. Wakatani, and A. J. Wooton: in *Ion Temper-*

ature Gradient Driven Turbulent Transport, (American Institute of Physics. New York. 1994)
3) T Kuroda, H. Sugama, R. Kanno, M Okamoto J Phys Soc Jpn **69** (2000) 2485
4) T. Kuroda, H Sugama, R. Kanno, M Okamoto Journal of Plasma Fusion Research SERIES **2** (1999) 105
5) G Rewoldt, L-P Ku, W. M Tang, H Sugama, N Nakajima, K Y Watanabe, S. Murakami, H Yamada, and W. A Cooper Phys. Plasmas **7** (2000) 4942.
6) G Rewoldt, L-P Ku, W M. Tang, and W A Cooper Phys Plasmas **6** (1999) 4705
7) J. L V Lewandowski: Plasma Phys. Control Fusion **40** (1998) 283
8) N Ohyabu,*et al* : J Plasma and Fusion Res **76**, 425 (2000)
9) A. Iiyoshi,*et al.*: Nucl Fusion **39** (1999)
10) H E. Mynick, T. K Chu, and A H Boozer Phys Rev. Lett **48** (1982) 322
11) K C. Shaing and S. A. Hoking: Phys. Fluids **26** (1983) 2136.
12) M. Wakatani. *Stellarator and Heliotron Devices* (Oxford University Press, 1998) p 271.
13) M. Yokoyama private communication
14) F. Romanelli, Phys. Fluids B **1** (1989) 1018.
15) J. Q. Dong, W Horton, and J. Y Kim Phys Fluids B **4** (1992) 1867
16) C Z. Cheng and K. T Tsang: Nucl Fusion **21** (1981) 643
17) P. H Rutherford and E. A Frieman. Phys. Fluids **11** (1968) 569.
18) J. B. Taylor and R J Hastie: Plasma Phys **10** (1968) 479
19) R. D. Hazeltine and J D. Meiss *Plasma Confinement* (Addison-Wesley, Redwood City, California, 1992) p. 298
20) R L Dewar and A. H Glasser Phys. Fluids **26** (1983) 3038
21) J. Y Kim, Y. Kishimoto, W. Horton, and T. Tajima, Phys. Plasmas **1** (1994) 927.
22) T. Kuroda, H. Sugama, R. Kanno, M. Okamoto, and W. Horton, J Phys. Soc. Jpn **67** (1998) 3787
23) H. Sugama: Phys. Plasmas **6** (1999) 3527.

Recent Issues of NIFS Series

NIFS-663 H Nakamura and T Sato H Kambe and K Sawada and T Saiki
Design and Optimization of Tapered Structure of Near-field Fiber Probe Based on FDTD Simulation Oct 2000

NIFS-664 N Nakajima,
Three Dimensional Ideal MHD Stability Analysis in L=2 Heliotron Systems Oct 2000

NIFS-665 S Fujiwara and T Sato,
Structure Formation of a Single Polymer Chain I Growth of trans Domains Nov 2000

NIFS-666 S Kida,
Vortical Structure of Turbulence Nov 2000

NIFS-667 H Nakamura, S Fujiwara and T Sato
Rigidity of Orientationally Ordered Domains of Short Chain Molecules Nov 2000

NIFS-668 I Mutoh, R Kumazawa, T Seki, K Saito, Y Torii, F Shimpo, G Nomura, I Watari, D A Hartmann, M Yokota, K Akaishi, N Ashikawa, P deVries, M Emoto, H Funaba, M Goto, K Ida, H Idei K Ikeda, S Inagaki, N Inoue, M Isobe, O Kaneko, K Kawahata, A Komori, T Kobuchi, S Kubo, S Masuzaki, T Morisaki, S Morita, J Miyazawa, S Murakamu, T Minami, S Muto, Y Nagayama, Y Nakamura, H Nakanishi, K Narihara, N Noda, K Nishimura, K Ohkubo, N Ohyabu, S Ohdachi, Y Oka, M Osakabe, T Ozaki, B J Peterson, A Sagara, N Sato, S Sakakibara, R Sakamoto H Sasao M Sasao, M Sato, T Shimozuma, M Shoji, S Sudo, H Suzuki, Y Takeiri, K Tanaka, K Toi, T Tokuzawa, K Tsumori, K Y Watanabe, T Watanabe, H Yamada, I Yamada, S Yamaguchi, K Yamazaki, M Yokoyama, Y Yoshimura, Y Hamada, O Motojima, M Fujiwara,
Fast- and Slow-Wave Heating of Ion Cyclotron Range of Frequencies in the Large Helical Device Nov 2000

NIFS-669 K Mima, M S Jovanovic, Y Sentoku, Z-M Sheng, M M Skoric and T Sato
Stimulated Photon Cascade and Condensate in Relativistic Laser-plasma Interaction Nov 2000

NIFS-670 L Hadzievski, M M Skoric and T Sato,
On Origin and Dynamics of the Discrete NLS Equation Nov 2000

NIFS-671 K Ohkubo, S Kubo H Idei, T Shimozuma, Y Yoshimura F Leuterer, M Sato and Y Takita,
Analysis of Oversized Sliding Waveguide by Mode Matching and Multi-Mode Network Theory Dec 2000

NIFS-672 C Das, S Kida and S Goto,
Overall Self-Similar Decay of Two-Dimensional Tirbulence Dec 2000

NIFS-673 L A Bureyeva, T Kato, V S Lisitsa and C Namba,
Quasiclassical Representation of Autoionization Decay Rates in Parabolic Coordinates Dec 2000

NIFS-674 L A Bureyeva, V S Lisitsa and C Namba,
Radiative Cascade Due to Dielectronic Recombination Dec 2000

NIFS-675 M F Heyn, S V Kasilov, W Kernbichler, K Matsuoka, V V Nemov S Okamura, O.S. Pavlichenko,
Configurational Effects on Low Collision Plasma Confinement in CHS Heliotron/Torsatron, Jan 2001

NIFS-676 K. Itoh,
A Prospect at 11th International Toki Conference - Plasma physics, quo vadis?, Jan 2001

NIFS-677 S Satake, H Sugama, M Okamoto and M Wakatani,
Classification of Particle Orbits near the Magnetic Axis in a Tokamak by Using Constants of Motion, Jan 2001

NIFS-678 M Tanaka and A Yu Grosberg,
Giant Charge Inversion of a Macroion Due to Multivalent Counterions and Monovalent Coions Molecular Dynamics Studyn, Jan. 2001

NIFS-679 K Akaishi, M Nakasuga, H Suzuki, M Iima, N Suzuki, A Komori, O Motojima and Vacuum Engineering Group,
Simulation by a Diffusion Model for the Variation of Hydrogen Pressure with Time between Hydrogen Discharge Shots in LHD, Feb 2001

NIFS-680 A Yoshizawa, N Yokoi, S Nisizima, S -I Itoh and K Itoh
Variational Approach to a Turbulent Swirling Pipe Flow with the Aid of Helicity, Feb 2001

NIFS-681 Alexander.A.Shishkin
Estafette of Drift Resonances, Stochasticity and Control of Particle Motion in a Toroidal Magnetic Trap, Feb 2001

NIFS-682 H Momota and G.H Miley,
Virtual Cathode in a Spherical Inertial Electrostatic Confinement Device, Feb 2001

NIFS-683 K Saito R Kumazawa, T Mutoh, T Seki, T Watari Y Torii, D A Hartmann Y Zhao A Fukuyama, F Shimpo, G Nomura, M Yokota, M Sasao, M Isobe, M Osakabe, T Ozaki K Narihara Y Nagayama, S Inagaki K Itoh, S Morita A V Krasilnikov, K Ohkubo, M Sato, S Kubo, T Shimozuma, H Idei, Y Yoshimura, O Kaneko, Y Takeiri, Y Oka K Tsumori K Ikeda A Komori H Yamada H Funaba K Y Watanabe S Sakakibara, M Shoji, R. Sakamoto, J Miyazawa K Tanaka B J Peterson N Ashikawa, S Murakami T Minami S Ohdachi S Yamamoto S Kado, H Sasao, H Suzuki, K Kawahata, P deVries, M Emoto H Nakanishi T Kobuchi N Inoue N Ohyabu Y Nakamura S Masuzaki S Muto, K Sato T Morisaki, M Yokoyama T Watanabe, M Goto I Yamada K Ida T Tokuzawa N Noda S Yamaguchi K Akaishi A Sagara K Toi K Nishimura, K Yamazaki, S Sudo Y Hamada, O Motojima, M Fujiwara,
Ion and Electron Heating in ICRF Heating Experiments on LHD Mar 2001

NIFS-684 S Kida and S Goto
Line Statistics Stretching Rate of Passive Lines in Turbulence Mar 2001

NIFS-685 R Tanaka, T Nakamura and T Yabe
Exactly Conservative Semi-Lagrangian Scheme (CIP-CSL) in One-Dimension Mar 2001

NIFS-686 S Toda and K Itoh,
Analysis of Structure and Transition of Radial Electric Field in Helical Systems Mar 2001

NIFS-687 T. Kuroda and H. Sugama,
Effects of Multiple-Helicity Fields on Ion Temperature Gradient Modes Apr 2001